Gen Shirane's Legacy in Polarized Beam Scattering: From Neutrons to X-rays

Martin BLUME[1,2], Doon GIBBS[2] and John HILL[2]

[1]*American Physical Society, Ridge, NY 11961, U.S.A.*
[2]*Brookhaven National Laboratory, Upton, NY 11973, U.S.A.*

We pay tribute to Gen Shirane's legacy by summarizing the results of x-ray magnetic scattering studies of a series of interesting materials, including chromium, NiO, MnF_2, rare earth boro-carbides, cuprates, and $NdNiO_3$ thin films. We focus on what may be learned through the use of polarization-dependent x-ray techniques, both elastic and inelastic, and compare that with the results of neutron scattering.

1. Introduction

In a famous paper published in 1959 Gen Shirane joined with Robert Nathans, Clifford Shull, and Arne Andresen in describing the production and use of monochromatic polarized neutrons.[1] This paper was among the first to explore the utility of using the polarization dependence of magnetic neutron scattering to extract detailed information on the magnetic behavior of solids. As such, it marked the start of a new field of neutron magnetic scattering, one that has seen remarkable growth over the intervening years, with large numbers of subsequent experiments and applications—including many by Gen himself.

In the late 1980's, the availability of modern synchrotrons as prodigious sources of x-rays sparked a similar expansion in the use of x-ray magnetic scattering as a realistic tool for the study of solid state magnetism. Driven in part by the awareness of the use of polarization effects by the neutron scattering community, the polarization dependence of the x-ray cross-section was quickly explored, and then exploited. In this endeavor, the present writers—admirers, colleagues, students, and friends of this great scientist—were influenced by Gen and his work in many ways. By way of a small tribute to him we mention in particular three papers which were inspired in part by Gen's work.[2–4] As was the case for neutron scattering, the use of polarized x-ray scattering has now become routine as a means to identify magnetic signals, to isolate magnetic scattering from the more ubiquitous charge scattering background and to extract detailed information on the spin order of the electrons in the solid. In this article, we summarize the x-ray magnetic scattering cross section and note a number of x-ray experiments in this area that we believe are particularly *a propos* to Gen, his work, and his legacy in the field of polarized beam scattering.

Interest in the use of x-ray scattering techniques to probe the magnetic structure and phase behavior of materials has continued to grow during the last two decades.[5] A significant effort has involved the continuing development and understanding of the techniques themselves, especially as ever-brighter x-ray beams have become available from modern synchrotron sources. Many classes of materials have been investigated—including rare earths, actinides, and transition metals—and in many forms: bulk elements and compounds; thin films, alloys and mutilayers; even surface layers. Today, one's perspective on the role of x-ray scattering in the study of magnetism is strikingly different than it was more than 30 years ago, when de Bergevin and Brunel reported the first x-ray magnetic scattering results on NiO obtained using a tube source.[6] Although not yet as mature as the field of neutron magnetic scattering, x-ray magnetic scattering is now associated with a diverse and impressive set of accomplishments.

The main factors driving the application of x-ray magnetic scattering techniques to materials center around the unique properties of synchrotron radiation. The high collimation of synchrotron beams, for example, has made possible ultra-precise measurements of the magnetic periods of antiferro-magnets and of large-length-scale critical fluctuations, which exist near magnetic ordering transitions, and the very high flux densities in small spots has allowed the inherently small cross-section to be overcome and very small volume samples to be studied.

Resonance magnetic scattering, which occurs when the incident x-ray energy is tuned near an absorption edge, has introduced species-sensitivity directly into the determination of magnetic structures. This is impossible by other scattering techniques. The well-defined polarization of the incident beam has opened new channels for determining magnetic structures, and permits the separation of spin and orbital magnetization densities in solids. Finally, the small beam size and high collimation have led to the increasingly common characterization of the magnetic structure and phase behavior of tiny samples, such as small particles, thin films, and surfaces.

It's worth adding here that although x-ray and neutron magnetic scattering techniques are analogous in many ways, their relative strengths are largely complementary. Neutron magnetic scattering remains a remarkably powerful probe of magnetic structure and phase behavior in single-crystal and powder samples, including both elastic and inelastic processes. Taken together, x-ray and neutron scattering add to the overall range of capabilities available for characterizing the microscopic magnetic properties of materials. The choice of technique depends solely on the details of the science to be studied. This is an idea that also guided Gen in his

research: one of his hallmarks was his ability to bring to bear the tools he needed to answer the particular question at hand.

2. Cross-section

The general cross section for elastic scattering of x-rays from a collection of atoms is

$$\left(\frac{d\sigma}{d\Omega}\right) = r_0^2 \left| \sum_n e^{i\boldsymbol{Q}\cdot\boldsymbol{r}_n} f_n(\boldsymbol{k},\boldsymbol{k}',\hbar\omega) \right|^2 \qquad (1)$$

where $r_0 = 2.8 \times 10^{-15}$ m is the classical electron radius, k and k' are the incident and scattered wavevectors of the photon, Q is the photon momentum transfer, and f_n represents the scattering amplitude from the nth atom. As derived within second-order perturbation theory,[5,7,8] this amplitude contains contributions sensitive to the magnetization at each site, which thus gives rise to x-ray magnetic scattering. Two limits of the magnetic scattering may be discerned from such an approach: resonant scattering (with the incident photon energy tuned near an absorption edge of a magnetic species in the sample) and nonresonant scattering (with the photon energy far from an absorption edge).

It is useful therefore to write

$$f_n(\boldsymbol{k},\boldsymbol{k}',\hbar\omega) = f_n^{\text{charge}}(\boldsymbol{Q}) + f_n^{\text{nonres}}(\boldsymbol{Q},\boldsymbol{k},\boldsymbol{k}') \\ + f_n^{\text{res}}(\boldsymbol{k},\boldsymbol{k}',\hbar\omega) \qquad (2)$$

where f^{charge} is the familiar Thomson scattering, f^{nonres} is the nonresonant magnetic scattering amplitude, and the resonant magnetic scattering amplitude is contained in the terms f^{res}. We consider the last two terms in detail below. The charge scattering is given by

$$f_n^{\text{charge}}(\boldsymbol{Q}) = -\rho_n(\boldsymbol{Q})\hat{\varepsilon}\cdot\hat{\varepsilon}' \qquad (3)$$

where ε (ε') is the incident (scattered) photon polarization state and $\rho_n(\boldsymbol{Q})$ the Fourier transform of the charge density. The scalar product of the polarization vectors implies that the polarization state is not rotated by charge scattering.

2.1 Nonresonant scattering

The nonresonant scattering amplitude may be written as[3,7]

$$f_n^{\text{nonres}}(\boldsymbol{Q}) = -i\frac{\hbar\omega}{mc^2}\langle M_{\text{nonres}}\rangle \\ = -i\frac{\hbar\omega}{mc^2}\left[\frac{1}{2}\boldsymbol{L}_n(\boldsymbol{Q})\cdot\boldsymbol{A} + \boldsymbol{S}_n(\boldsymbol{Q})\cdot\boldsymbol{B}\right] \qquad (4)$$

where $\langle M_{\text{nonres}}\rangle$ is the magnetization-dependent part of the amplitude, and $\boldsymbol{L}_n(\boldsymbol{Q})$ and $\boldsymbol{S}_n(\boldsymbol{Q})$ are the Fourier transforms of the orbital and spin magnetization densities at the nth atom, respectively. The vectors A and B contain the polarization dependencies of these two contributions to the scattering. Importantly, the two vectors are not equal and have distinct Q dependencies. This allows the ordered L and S moments of the system to be obtained separately by measuring the polarization of the scattered beam for a number of magnetic reflections. Expressions for A and B may be found in the literature.[7]

For experiments with linear incident polarization, the scattering amplitudes are most usefully expressed in terms of linear polarization basis states.[3] For nonresonant magnetic scattering,

$$\langle M_{\text{nonres}}\rangle = \begin{pmatrix} \langle M_{\sigma\sigma}\rangle & \langle M_{\pi\sigma}\rangle \\ \langle M_{\sigma\pi}\rangle & \langle M_{\pi\pi}\rangle \end{pmatrix} \\ = -i\left(\frac{\hbar\omega}{mc^2}\right)\begin{pmatrix} \sin 2\theta S_2 & -2\sin^2\theta[\cos\theta(L_1+S_1)-\sin\theta S_3]_i \\ 2\sin^2\theta[\cos\theta(L_1+S_1)+\sin\theta S_3] & \sin 2\theta[2\sin^2\theta L_2 + S_2] \end{pmatrix} \qquad (5)$$

in the coordinate system of Fig. 1. σ and π refer to the linear polarization states perpendicular and parallel to the scattering plane, respectively, and 2θ is the scattering angle. For linear incident polarization, the $\sigma \to \sigma$ scattering is given by $|\langle M_{\sigma\sigma}\rangle|^2$, the $\sigma \to \pi$ scattering by $|\langle M_{\sigma\pi}\rangle|^2$, and so on. In this same basis, the amplitude for charge scattering is diagonal:

$$f_n^{\text{charge}}(\boldsymbol{Q}) = -\rho(\boldsymbol{Q})\begin{pmatrix} 1 & 0 \\ 0 & \cos 2\theta \end{pmatrix}. \qquad (6)$$

As a result of the small prefactor $\hbar w/mc^2$, nonresonant magnetic scattering is weak relative to charge scattering. A rough estimate of the ratio of the magnetic to the charge scattering is

$$\left|\frac{f_n^{\text{nonres}}}{f_n^{\text{charge}}}\right|^2 \sim \left(\frac{\hbar\omega}{mc^2}\right)^2 \left(\frac{F_m}{F_c}\right)^2 |\langle S\rangle^2| \left(\frac{N_m}{N}\right)^2 \qquad (7)$$

where F_m and F_e are the magnetic and charge form factors, $\langle S\rangle$ is the ordered spin of one electron, and N_m/N is the ratio of the number of magnetic to total electrons. For typical x-ray energies between 5 and 10 keV this ratio is about 1×10^{-5}; however, in practice it is rarely larger than 1×10^{-6} even in the most favorable cases.

2.2 Resonant scattering

Resonant scattering arises from second-order scattering processes. They may be thought of as corresponding to the absorption of an incident photon, the creation of a short-lived intermediate (excited) state, and the decay of that state back into the ground state via the emission of an elastically scattered photon. For Bragg scattering, this process is coherent. A schematic energy-level diagram illustrating resonant scattering for a rare earth ion at the L_3 absorption edge is shown in Fig. 2.
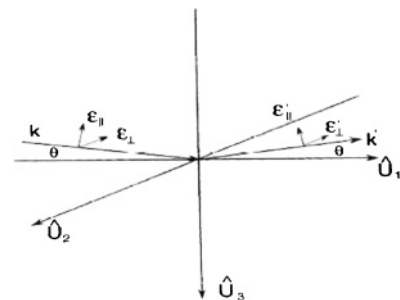

Fig. 1. Coordinate system used in this chapter. Note that the momentum transfer Q is along –U3. (After Blume and Gibbs 1988.[3])
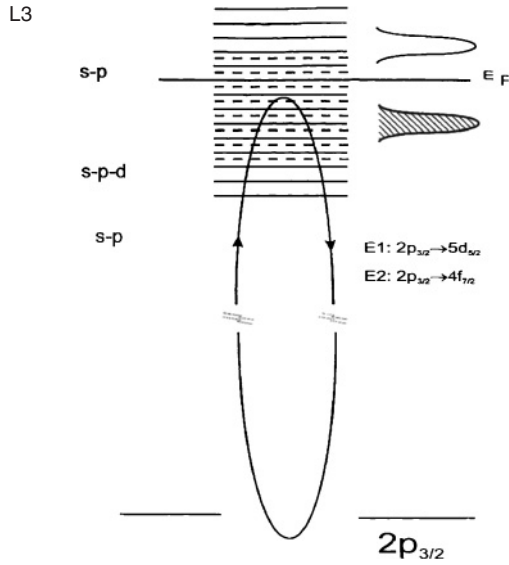
Fig. 2. Schematic single-electron picture of the resonant scattering process, illustrated for a rare earth, at L_3 edge. A $2p_{3/2}$ electron is excited into an unoccupied state above the Fermi level by the incident photon. The $5d$ states are reached through electric dipole transitions and the $4f$ through electric quadrupole transitions. In the elemental rare earths, the $5d$ states form delocalized bands, polarized through an exchange interaction with the localized, magnetic $4f$s. Resonant elastic scattering results when the virtually excited electron decays by filling the core hole and emitting a photon (from Gibbs 1992[9]).

$$f_n^{\text{res}}(\boldsymbol{k}, \boldsymbol{k}', \hbar\omega)$$

$$= -\frac{1}{m}\sum_c \left(\frac{E_a - E_c}{\hbar\omega}\right) \frac{\langle a|O_\lambda(\boldsymbol{k})|c\rangle\langle c|O_{\lambda'}^\dagger(\boldsymbol{k}')|a\rangle}{E_a - E_c - \hbar\omega}$$

$$+ \frac{1}{m}\sum_c \left(\frac{E_a - E_c}{\hbar\omega}\right) \frac{\langle a|O_{\lambda'}^\dagger(\boldsymbol{k}')|c\rangle\langle c|O_\lambda(\boldsymbol{k})|a\rangle}{E_a - E_c + \hbar\omega - \mathrm{i}\frac{\Gamma}{2}} \quad (8)$$

where E_a, $|a\rangle$ and E_c, $|c\rangle$ are the energies and wavefunctions of the initial and intermediate states of the system, respectively, Γ is the inverse lifetime of the intermediate state, k and k' are the incident and scattered photon wavevectors, respectively, and m is the rest mass of the electron. The operator $O_\lambda(\boldsymbol{k})$ is given by

$$O_\lambda(\boldsymbol{k}) = \sum_i e^{\mathrm{i}\boldsymbol{k}\cdot\boldsymbol{r}_i}(\boldsymbol{P}_i \cdot \hat{\varepsilon}_\lambda - \mathrm{i}\hbar\hat{\varepsilon}_\lambda \cdot (\boldsymbol{k} \times \boldsymbol{S}_i)) \quad (9)$$

where λ indexes the incident (scattered) photon polarization $\hat{\varepsilon}_\lambda$ ($\hat{\varepsilon}_\lambda'$), $\boldsymbol{P}_j$ and $\boldsymbol{S}_j$ are the momentum and spin of the ith electron, respectively, and the index i runs over all of the electrons at site n. The two terms in eq. (8) contain all the dependence of the scattering on the incident photon energy. As an aside, we note that these are also the terms that give rise to x-ray magnetic circular dichroism (XMCD) in the limit of zero momentum transfer.[8]

In a resonant x-ray scattering experiment, the incident photon energy $\hbar\omega$ is tuned to the vicinity of an absorption edge (i.e., $\hbar\omega = E_c - E_a$). If the second, resonant, term in eq. (8) depends on the magnetization at site n, it can give rise to magnetic scattering. This is the case if, for example, the intermediate energy levels are exchange split, producing shifts in the resonant denominator, or if the overlap integrals depend on the net magnetic polarization.[10] In general, such

sensitivity arises from spin–orbit correlations, which must be present in at least one of the two levels involved in the resonance, and from exchange effects. If the momentum transfer is set to a magnetic wavevector, the sum over intermediate states is then nonzero, and this leads to resonant magnetic scattering. That resonant scattering is sensitive to the magnetization was first suggested by Blume[7] and observed in Ni metal by Namikawa *et al.*[11] It was explored in detail by Hannon *et al.*[10] following the observation of large enhancements at the L-edges of Ho.[12] The largest resonant enhancements observed to date have occurred at actinide M_4 absorption edges (e.g., ref. 13).

Until recently, all the experimental phenomena observed by resonant magnetic scattering have been explained satisfactorily in terms of a one-electron description of electric multipole transitions.[10,14] In this picture, the size of the resonant enhancement of the magnetic scattering depends on a combination of factors, including the radial matrix elements ($\langle c|r^L|a\rangle$, where $L = 1, 2, \ldots$ for dipole, quadrupole, ... transitions), the magnetic polarization of the intermediate state, the value of the intermediate state lifetime, and the energy width of the incident photon. The 4-orders-of-magnitude (and larger) enhancements observed at the M_4 and M_5 edges in the actinides[13] are then a result of the strong dipole transitions, which couple directly to the magnetic $5f$ electrons ($d \to f$). Similarly, the 10- to 100-fold enhancements observed at the L_2 and L_3 edges of the rare earths[12,15–18] are explained in terms of the smaller overlap integrals and weaker magnetization of the $5d$ levels as reached in the dipole process, $2p \leftrightarrow 5d$. It turns out that electric quadrupolar transitions may also be significant, for example, at the rare earth $L_{2,3}$ edges. These couple to the magnetic $4f$ levels, via $2p \leftrightarrow 4f$. Such scattering is typically weaker because of the still smaller matrix elements. In Ho, for example, quadrupole scattering was observed to be approximately 5 times weaker than the dipole scattering at the first harmonic.[15]

In contrast to nonresonant x-ray and neutron magnetic scattering, resonant x-ray scattering does not contain a magnetic form factor. This results from the two-step nature of the resonant scattering process. Specifically, in the formula for the scattering [eq. (8)], k and k' always appear independently, and the expression cannot be reduced to a function of their difference, $\boldsymbol{Q}$. Thus, there is no Fourier transform of the magnetization density of the nth site, as there is for the nonresonant magnetic scattering [eq. (4)].

The polarization dependence of the resonant scattering is a function of moment direction and scattering geometry. In the basis of Fig. 1, the dipole (El) scattering has the form:[4,10,19]

$$f_{nE1}^{\text{XRES}} = \langle M_{\text{res}}\rangle =$$

$$= F^{(0)}\begin{pmatrix} 1 & 0 \\ 0 & \cos 2\theta \end{pmatrix}$$

$$- \mathrm{i}F^{(1)}\begin{pmatrix} 0 & z_1\cos\theta + z_3\sin\theta \\ z_3\sin\theta - z_1\cos\theta & -z_2\sin 2\theta \end{pmatrix}$$

$$+ F^{(2)}\begin{pmatrix} z_2^2 & -z_2(z_1\sin\theta - z_3\cos\theta) \\ +z_2(z_1\sin\theta + z_3\cos\theta) & -\cos^2\theta(z_1^2\tan^2\theta + z_3^2) \end{pmatrix}.$$

$$(10)$$

The z_j are the components of a unit vector along the quantization axis at site n; the $F^{(L)}$ are the resonant matrix elements (see ref. 10). The first term contains no dependence on the magnetic moment and therefore contributes only to the charge Bragg peaks. The second term is linear in z, and for an antiferromagnet will produce new scattering at the magnetic wavevector. The final term is quadratic in z. This will produce scattering at twice the ordering wavevector, leading to a second-order *resonant* harmonic.

As an example, the scattering of linearly polarized σ_i radiation from a magnetic spiral gives rise to a first harmonic with integrated intensity varying as[4]

$$\left.\frac{\mathrm{d}\sigma}{\mathrm{d}\Omega}\right)^{\mathrm{XRES}}_{\mathrm{E1}} = \frac{1}{4}\cos^2\theta |F^{(1)}|^2 \delta(\boldsymbol{Q}-\boldsymbol{G}\pm\tau) \qquad (11)$$

The integrated intensity of the second harmonic varies as

$$\left.\frac{\mathrm{d}\sigma}{\mathrm{d}\Omega}\right)^{\mathrm{XRES}}_{\mathrm{E1}} = \frac{1}{16}(1+\sin^2\theta)|F^{(2)}|^2\delta(\boldsymbol{Q}-\boldsymbol{G}\pm2\tau) \qquad (12)$$

In these expressions, $\boldsymbol{G}$ is a reciprocal lattice vector and τ the spiral wavevector. For the case of the second harmonic, there is both $\sigma \to \sigma$ and $\sigma \to \pi$ scattering, where for the first harmonic, there is only a $\sigma \to \pi$ component.

The situation for quadrupole transitions is more complex.[4,10] Terms up to $O(z^4)$ are obtained in the cross section, giving rise to up to four higher, resonant harmonics. Second- and higher-order resonant harmonics (both dipole and quadrupole) are practically observable only in incommensurate systems, for which there is no overlap with the bulk Bragg peaks.

The original formulation of the resonant cross section by Hannon *et al.*,[10] has been re-expressed in terms of effective scattering operators following the theoretical development of the cross section for x-ray magnetic circular dichroism (XMCD).[14,20–22] These operators relate the resonant elastic and inelastic scattering cross sections directly to the orbital and spin magnetization densities, among other physically interesting properties of the system, and will lead to sum rules for diffraction experiments analogous to those that have been derived for magnetic circular dichroism. It is also worth adding that there has been increasing interest in examining and using K-edge resonances ($s \leftrightarrow p$) in x-ray magnetic scattering experiments.[23–26] Obviously, the current understanding of x-ray resonant magnetic scattering, which is based primarily on the spin–orbit splitting of the core level, does not apply here. Indeed, the presence of K-edge resonances implies the existence of spin–orbit splitting in the intermediate states, which itself has become a topic of interest. Finally, we note that experiments carried out at the Dy L edges of $DyFe_4Al_8$[27] suggest a failure of the one-electron atomic picture of resonant scattering—in particular, they suggest that band structure effects are important. In addition, the observation of resonant enhancements from non-magnetic ions[28] has also led to questioning of our understanding of the resonant cross-section.[29,30] It seems likely that there will continue to be further discussion of the x-ray cross section in the coming years.

3. Spin and Orbital Magnetization Densities

The first applications of x-ray magnetic scattering techniques were made by de Bergevin and Brunel in nonresonant studies of of NiO, Fe_2O_3, and Fe.[6,31] They had already recognized that a special feature of the non-resonant cross section involved the possibility of distinguishing the orbital and spin magnetization densities on the basis of their polarization dependencies.[31,32] The ideas are most simply illustrated by considering the nonresonant magnetic scattering from a simple spiral magnetic structure. Under the assumption of purely linear incident polarization, σ, and scattering along the (00L) axis (Fig. 1), the cross section for pure, non-resonant, magnetic scattering from a perfect spiral has the following form:[3]

$$I'_\sigma \sim |\boldsymbol{S}(Q)|^2$$

and

$$I'_\pi \sim |\boldsymbol{L}(Q)+\boldsymbol{S}(Q)|^2 \qquad (13)$$

where I'_σ and I'_π are σ and π polarized intensities (linear unrotated and rotated. respectively) of the magnetic scattering. $\boldsymbol{S}(Q)$ and $\boldsymbol{L}(Q)$ represent the respective Fourier transforms of the spin and orbital angular magnetization densities evaluated at $\boldsymbol{Q}$. It is clear that by measuring the σ and π polarized magnetic scattering intensities from a spiral versus momentum transfer, it is possible to deduce the Q-dependence of the orbital and spin magnetization densities separately. These kinds of experiments turn out to be extremely challenging, requiring near-perfect incident polarization and quantitative polarization analysis of the scattered beam. Successful but qualitative experiments have been carried out on second-generation sources in studies of the rare earth metal holmium.[12,15] In that work it was possible to show that the orbital magnetization density provided the dominant contribution to the π-polarized component of the magnetic scattering, consistent with expectations in holmium (for which $L = 6$ and $S = 2$). However, it was not possible to obtain a reliable determination of the $\boldsymbol{Q}$-dependence of the spin and orbital angular momentum densities. The experimental difficulties owed in large part to the imperfectly linear polarization and large horizontal divergence of the incident beam. The latter is important since quantitative polarization analysis of the scattered beam requires that the scattered σ and π polarized intensities (which are in and out of the diffraction plane, respectively) be collected with equal efficiencies.

These hurdles are naturally overcome at synchrotron sources, for which the incident linear polarization is well defined and the vertical and horizontal divergences are well matched. Moreover, the high degree of incident linear polarization has led to the construction of diamond and Si quarter-wave plate instrumentation,[33,34] which allow the incident polarization to be arbitrarily tuned. This increases enormously the flexibility possible in choosing geometries for separating the orbital and spin densities and will be especially important in applications to ferromagnets.[3,35]

An example of this type of application is shown for NiO in Fig. 3. NiO is a $3d$ transition element monoxide with a face-centered-cubic crystal structure and a type II antiferromagnetic structure below 523 K. The $3d$ electrons of the transition metals are extremely sensitive to the crystal field, and in contrast to the case of rare earths discussed above, the orbital momentum is largely quenched. Traditionally, the fraction of orbital momemtum comprising the total magnet-
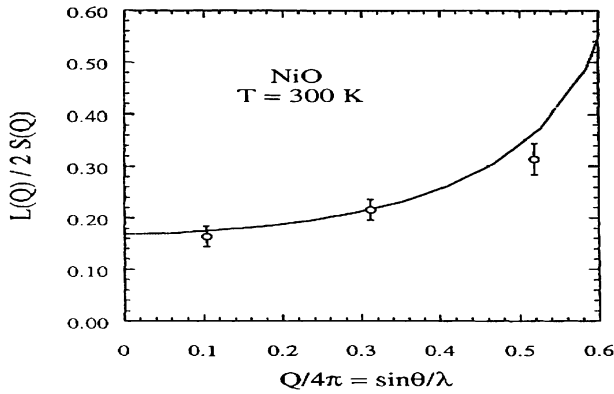
Fig. 3. Measured variation of $L(Q)/2S(Q)$ as a function of $\sin\theta/\lambda = Q/4\pi$. The continuous line is the Q-dependence estimated theoretically and adjusted to fit through the data with a contraction of the wavefunction by 17%. (From Fernandez *et al.* 1998.[36])

Fig. 4. (a) The intensity variation of the x-ray magnetic scattering observed at the $(2 - Q, 0, 0)$ satellite in chromium. At $T_{SF} = 122$ K, the transverse polarization of the SDW is transformed to a longitudinal polarization. The sudden decrease in intensity observed here reflects the polarization dependence of the non-resonant x-ray cross-section. Open circles were taken on warming, closed circles on cooling. (b) The scattering geometry. Q is the modulation wave-vector and is parallel to the scattering vector. In the transverse SDW phase the polarization is perpendicular to Q and the scattering is dominated by the component S'. In the longitudinal SDW phase ($T < T_{SF}$), the polarization S is along Q. Figure taken from ref. 38.

izization has been detected through either paramagnetic resonance measurements of g factors or through polarized neutron scattering determinations of the magnetic form factor (again in the paramagnetic phase). However, these methods do not provide information about the magnetically ordered phase. The ratio of the spin and orbital form factors, as deduced by x-ray magnetic scattering from NiO, is plotted versus the momentum transfer Q in Fig. 3.[36] Extrapolating to $Q = 0$ gives an $L/2S$ ratio of 0.17, which is surprisingly large. By placing the scattered intensities on an absolute scale, the spin and orbital momentum contributions to the total staggered magnetization in NiO were found to be $S = 0.95 \pm 0.1\mu_B$ and $L = 0.32 \pm 0.05\mu_B$. The total magnetic moment is about $2.2 \pm 0.2\mu_B$ at 300 K, which is close to the value determined by neutron scattering ($1.9 \pm 0.2\mu_B$). The analysis of the Q-dependence of the magnetic form factors further indicates a contraction of the electronic wavefunctions similar to that observed with neutrons.[37]

4. Spin Density Waves in Chromium

Chromium is the canonical spin density wave system and, not incidentally, a problem dear to Gen's heart for many years. As a result of Fermi surface nesting, it forms an incommensurate, transverse spin-density wave (TSDW) below a Neel temperature of $T_N = 311$ K. The incommensurability, δ, varies from $\delta = 0.037$ r.l.u. at T_N, to $\delta = 0.048$ r.l.u. at $T = 10$ K. At $T = T_{SF} = 122$ K, the SDW undergoes a spin-flip transition, in which the polarization rotates to become parallel to the modulation wave vector and a longitudinal SDW (LSDW) forms. In 1995, two of the present authors carried out the first x-ray magnetic scattering studies of chromium, observing the transverse spin density wave.[38] On cooling below T_N, the intensity was observed to grow, until at $T = T_{SF}$ there was an abrupt decrease in the scattering which dropped to below detectable levels at low temperatures (Fig. 4).

This was understood in terms of the polarization dependence of the non-resonant x-ray scattering cross-section—which is most sensitive to the component of the spin perpendicular to the scattering plane [eq. (5)]. These data revealed that the magnetic correlation length for the SDW magnetic order was well in excess of 4000 Å. [In a historical aside, we note that Gen Shirane visited the x-ray beamline
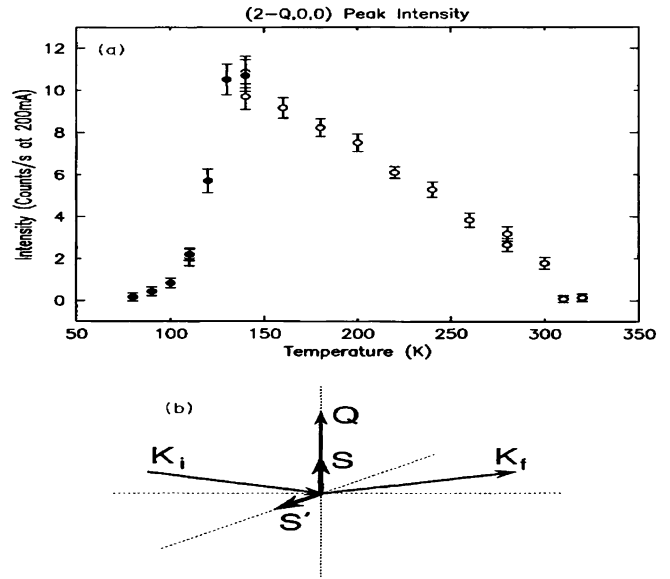
the day these data were taken and instantly understood this effect based on his intuition developed from years of working with the neutron magnetic cross-section.]

In recent developments, these antiferromagnetic domains have now been imaged directly using x-ray magnetic scattering.[39] Evans *et al.* illuminated the sample with an x-ray spot 5000Å across and then measured the x-ray magnetic scattering intensity as a function of spot position. Domains several tens of microns across were imaged (Fig. 5). Further, on cooling into the LSDW phase, the transition was observed to occur commencing at the domain walls first (Fig. 5); that is the magnetic phase boundary nucleated the LSDW phase.[39]

Perhaps the most important implication of these results is that they point to the use of polarization effects in the x-ray magnetic scattering cross-section as a means of imaging antiferromagnetic domains—a topic of significant interest as antiferromagnetic materials become increasingly important in technologically relevant materials.

5. Magnetic Moment Direction Determination

As Nathans *et al.* noted in their early paper,[1] the use of polarization dependent neutron scattering allows one to determine the moment direction uniquely. Similar determinations are in principle possible with x-rays. Early work in this x-ray magnetic structure solving technique was performed by Detlefs *et al.*[40,41] utilizing resonant x-ray scattering. The ability of x-ray resonant scattering to determine moment directions has great utility for materials not amenable to neutron scattering techniques, either because they have very large neutron absorption cross-
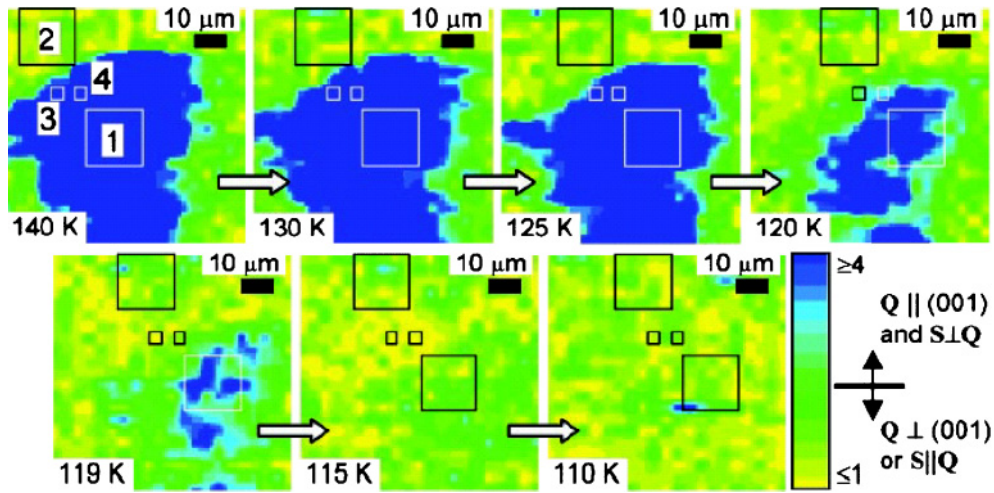
Fig. 5. (Color online) Images of a single TSDW domain at temperatures near TSF. The transition from transverse to longitudinal spin polarization at TSF results in the disappearance of x-ray magnetic scattering from the SDW domain. Figure from ref. 39.

sections (Sm, Gd, ...) or because the available samples are too small. In addition, the element specificity of the technique makes it particularly interesting for mixed spin systems, since, in principle, it is possible to determine the temperature dependence and ordered moment direction of each sublattice with a model-independent procedure, in contrast to neutron-scattering methods. In addition, x-ray resonant scattering offers the ability to study surface magnetism, and the potential to resolve orbital and spin contributions through the use of sum rules.

In 1996, Detlefs *et al.*[40] demonstrated that it was possible to determine moment directions using only resonant x-ray magnetic scattering. They studied two related compounds, $NdNi_2B_2C$ and $SmNi_2B_2C$, both of which order in a commensurate antiferromagnetic structure with propagation vector $(1/2, 0, 1/2)$.

The experiments were carried out at beamline X22C of the National Synchrotron Light Source with the samples mounted in a closed cycle refrigerator such that the $(h0l)$ zone was coincident with the diffraction plane. The integrated intensity was measured for a series of magnetic reflections (Fig. 6). These data were taken in each of the two samples at the respective rare-earth L_2 edges. These resonances are dominated by the dipole $2p_{3/2}$–$5d$ transitions. For $NdNi_2B_2C$, the moment direction was previously known to be along the (100) direction, and the integrated intensity was well modeled by such a description (top panel, Fig. 6). For $SmNi_2B_2C$, the moment direction was not known. The model simulations suggested that there was no a-axis component, but that there was a finite c-axis component to the ordered moment. However, as a consequence of the particular geometry used, the dipole resonant scattering was insensitive to the b-axis component, and so these measurements did not result in a complete determination of the moment direction. The authors then utilized the L_3 resonance, for which a significant quadrupole $(2p$–$4f)$ resonance was observed. Such quadrupolar scattering has a different polarization dependence than the dipole scattering[4] and thus by studying this it was possible to determine that the moment direction was in fact along the (001) direction (Fig. 7). This work was the first x-ray determination of
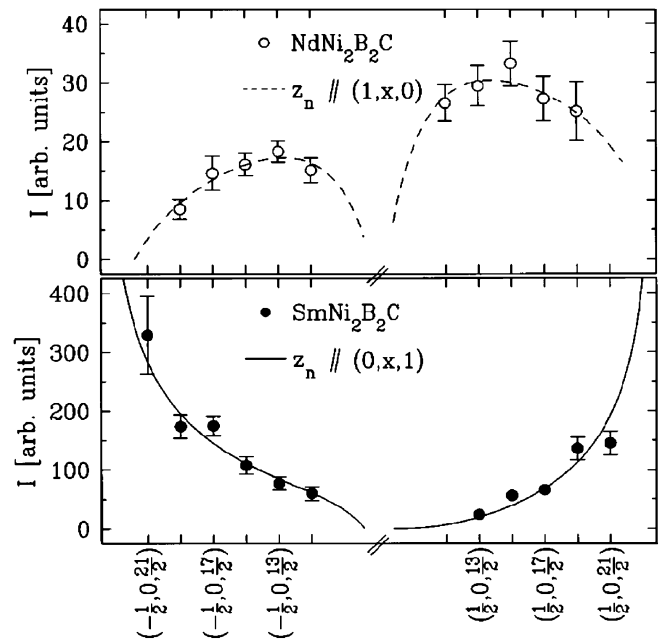

Fig. 6. The integrated intensity of the magnetic reflections of $SmNi_2B_2C$ (closed symbols) and $NdNi_2B_2C$ (open symbols) along with model calculations for a magnetic moment parallel to the c (—) and a (- - -) axes of the samples. The data were taken at the respective rare-earth L_2 (dipole) edges of the two compounds. The symbol cross not x denotes the fact that these measurements are not sensitive to components of the magnetic moment along the b-axis of the samples. Figure taken from ref. 41.

moment direction with no *a priori* information, and in that sense is reminiscent of the 1959 paper by Nathans, Shull, Shirane, and Anderson.[1]

6. Soft X-ray Resonant Scattering

The utility of polarization dependent measurements of x-ray scattering, and in particular, resonant x-ray scattering, has only continued to grow following these early measurements—again mirroring the equivalent growth in the neutron community sparked by the classic work of Nathans, Shull, Shirane, and Andresen. In recent years, the x-ray work has been extended in any number of directions including, surface
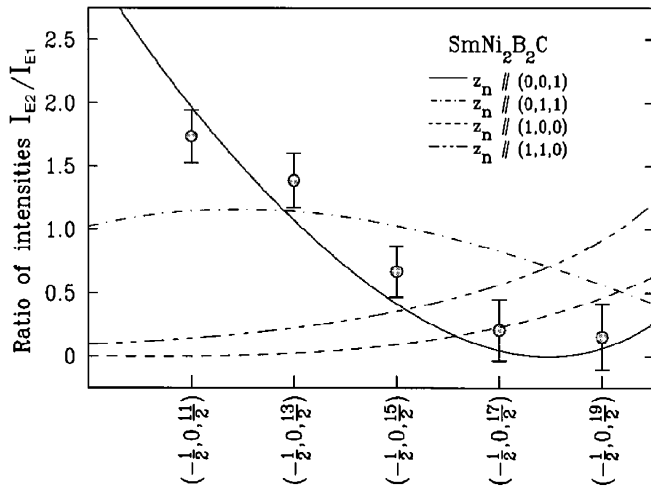
Fig. 7. The ratio of the intensities of dipolar and quadrupolar scattering at the Sm L3 edge in $SmNi_2B_2C$, along with model calculations for several directions of the magnetic moments. The simulations show that there can be no significant *b*-axis component to the ordered moment and that the moment direction is therefore purely along the *c*-axis. Figure taken from ref. 41.

x-ray scattering, scattering in high magnetic fields, scattering from thin films and most recently from other types of electronic order (including charge order and orbital order). In this example, we make note of the recent explosion of activity in the soft x-ray region (specifically working at the transition metal L-edges) and describe some recent work of Scagnoli *et al.*[42]

In this work, the authors utilized the Ni $L_{2,3}$ edges to study the magnetism in $NdNiO_3$ films. This compound exhibits a temperature driven metal–insulator transition at $T_{MI} = 200$ K. Antiferromagnetic order sets in at the same temperature. By varying the incident and final polarization, and studying the azimuthal dependence of the scattering (that is the dependence on rotation about the scattering vector), they were able to show that the scattering at the magnetic wave-vector was purely magnetic and did not, for example, also arise from orbital ordering of the Ni 3*d*

electrons. Polarization analysis of the scattered beam confirmed this interpretation. Further, in contrast to earlier neutron diffraction studies, which could not unambiguously determine the magnetic structure, the resonant soft x-ray scattering results show that the magnetic structure is non-collinear (Fig. 8). In addition, calculations of the resonance profile show that the two features observed in the spectra can be associated with Ni^{2+} and Ni^{3+} contributions, that is, the compound exhibits charge disproportion (in agreement with earlier resonant hard x-ray diffraction). Taken together, these results show that in this material, the metal–insulator transition is solely driven by charge disproportion. From a broader point of view, this work illustrates a way in which the dependence of polarization of x-ray scattering is distinct from neutron scattering and opens new possibilities for understanding magnetic, orbital and charge ordering in many materials.

7. High Energy Limit

In the opposite extreme, another new direction for x-ray magnetic scattering studies, which has grown during the last two decades, involves the use of high-energy x-ray beams from 80 up to nearly 500 keV. There are a number of clear advantages available in this regime in comparison to lower-energy nonresonant and resonant x-ray magnetic scattering. Most prominently, the x-ray penetration depth at 100 keV, or higher, is typically of order 1 mm for most materials. As a result, high-energy x-ray scattering experiments are generally carried out in a transmission geometry, analogous to netron scattering. It follows that unlike most other x-ray scattering experiments in the range 8 to 20 keV, high-energy experiments probe the entire bulk of the sample. This implies that surface effects, for example, which may exist over depths of up to several micrometers, depending on surface preparation, are easily avoided. Indeed, they can often be identified directly and characterized in relation to the bulk properties by this method. In addition, there is a volume enhancement of the magnetic signal, which can increase the magnetic signal by orders of magnitude. The latter is compensated by the λ^3 dependence of the diffraction
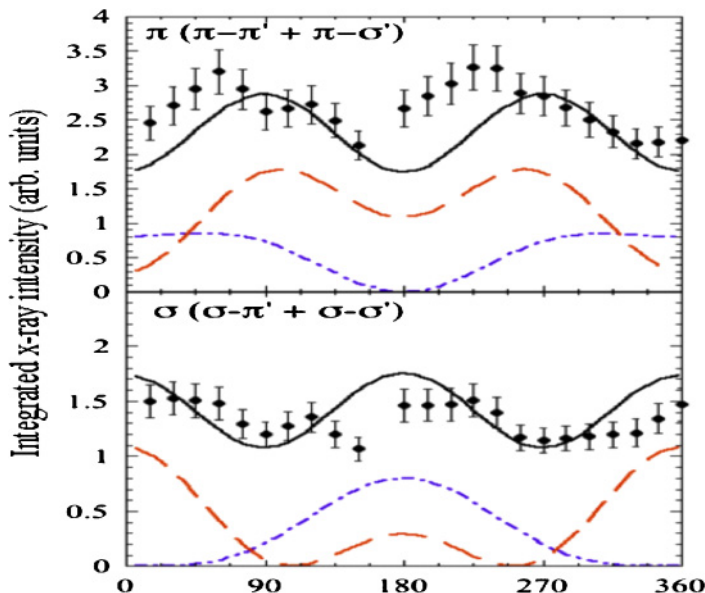

Fig. 8. (Color online) Integrated intensity of the $(1/2, 0, 1/2)$ reflection at $T = 30$ K as a function of azimuthal angle taken at 857.4 eV (Ni L3 edge) with Π (upper panel) and σ (lower panel) incident radiation. The solid line corresponds to the calculations for a non-collinear magnetic model. The dotted and dashed lines represent the collinear models with moments along the a axis and within the (a, c) plane respectively. $\psi = 0°$ is for [010] along the *z*-axis. Figure taken from ref. 42.
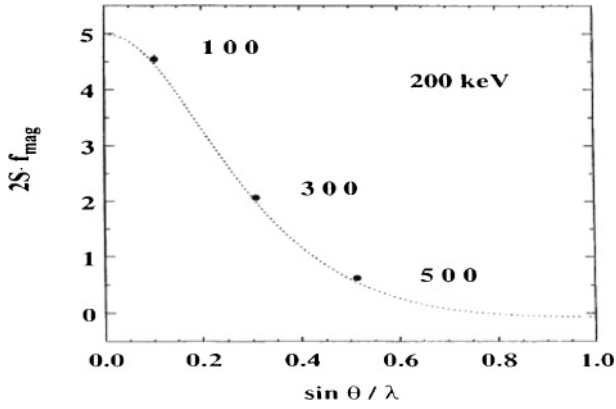
Fig. 9. Magnetic structure factor of MnF_2 measured at 200-keV photon energy. The dashed line represents the magnetic structure facture calculated with the magnetic form factor for Mn^{2+}. (From ref. 46)

cross section, however, resulting in a net enhancement of between 10 and 100 in favorable cases. This is especially important in transition metal compounds, for which no L or M absorption edges fall conveniently within the range 3 to 20 keV. Signal rates reaching 20,000 s^{-1} have been obtained at the magnetic reflections of MnF_2[43] in experiments carried out at 80 keV. This has led to an extremely precise characterization of the exponent describing the reduced temperature dependence of the magnetic order parameter.[43] Another striking recent example of the use of high-energy x-ray scattering is the observation of charge and (possibly) magnetic stripe order in high-T_c superconducting cuprates and nickelates. These studies confirmed similar observations made by neutron scattering[44,45] and lend support to a stripe-phase description of high-temperature superconductors.

There is another property of high-energy x-ray magnetic scattering that can be used to advantage in x-ray magnetic scattering studies: namely, that the nonresonant high-energy cross section is considerably simpler than either that of the resonant or lower energy nonresonant cross sections. In the limit as $\hbar\omega > \sim 100$ keV, the magnetic intensity reduces to $|S_\perp|^2$, where $S_\perp$ is the component of the spin magnetization density perpendicular to the diffraction plane. This polarization dependence enormously simplifies subsequent magnetic structure analysis, and leads directly to the determination of the Q-dependence of the spin form factor. It also offers a useful starting point for isolating the spin and orbital magnetization densities when complemented with low-energy nonresonant x-ray scattering or neutron scattering studies of the orbital and spin densities. The Q-dependence of the magnetic form factor of MnF_2 obtained at 200 keV is shown in Fig. 9.[46] These data are in excellent agreement with neutron diffraction determinations published earlier. In this regard, it is interesting to note that Strempfer *et al.*[46] also verified that as $\hbar\omega \to mc^2$, where the approximations underlying the derivation of the x-ray magnetic cross section break down, the high-energy cross-section nevertheless remains a useful description of the magnetic scattering.

8. Resonant Inelastic X-ray Scattering

One particular strength of neutron scattering is the ability to perform inelastic measurements to study the excitation spectra of condensed matter systems. This was something Gen was a master at exploiting in utilizing triple axis neutron spectrometers to study a wide variety of excitations. Here, neutrons have an intrinsic advantage because the energy of thermal neutrons is well matched to excitations of interest in condensed matter.

In contrast, for x-rays, the energy of a 1 Å photon is 12 keV, 5 to 6 orders of magnitude larger than energies of interest in solid state systems. Thus, to study relevant excitations, very high resolutions are required, on the order of 1 part in 10^5 and higher, and result in a consequent large reduction in the incident flux (leaving aside the technical challenges of achieving such a resolution). Here, just as was the case for magnetic x-ray scattering, the enormous brightness of synchrotron sources has made up this deficit and inelastic measurements have now been performed in a wide variety of systems. This field too has seen enormous progress in the last five to ten years and while he never carried out an inelastic x-ray scattering experiment, it was a field that Gen actively encouraged and believed in—indeed he even invested in some of the early instruments used in the field at the National Synchrotron Light Source (NSLS).

In another parallel with x-ray magnetic scattering, it turns out that it is again useful to take advantage of resonances in the cross-section to enhance the scattering. In fact, such resonances were first observed in the hard x-ray regime by C.-C. Kao and co-workers[47] using the instrument mentioned above. Formally, the resonant inelastic scattering process may be written down as:

$$F(\Omega, \omega)$$
$$= \sum_j \left| \sum_i \frac{\langle j|T|i\rangle\langle i|T|g\rangle}{E_g + \Omega - E_i - i\Gamma} \right|^2 \delta(E_g + \Omega - E_j - \omega), \quad (14)$$

where $|g\rangle$ is the ground state of the Hamiltonian H with energy E_g, and $|i\rangle$ (with energy E_i) and $|j\rangle$ (with energy E_j), are the intermediate and final states, respectively. The operator T represents the (dipole) radiative transition. Ω and ω, are, respectively, the incident and emitted photon energies, and Γ represents the spectral broadening due to the core–hole lifetime in the intermediate state.

A schematic of the process is shown in Fig. 10 for the case of a copper ion in a cuprate. Here, it is well known that in the CuO planes, the Cu $3d^9$ configuration hybridizes with the $3d^{10}$ $\underline{L}$ configuration, where $\underline{L}$ represents an O $2p$ ligand hole of finite bandwidth. Within the Anderson impurity model, this results in discrete bonding and anti-bonding states composed of a mixture of $3d^9$ and $3d^{10}$ $\underline{L}$ configurations, with a continuous band between them (Fig. 10). The ground state is then the bonding state, with about 60% $3d^9$. The lowest edge of the continuous band (charge transfer gap) is typically about 2 eV above this and the anti-bonding state is ∼6 eV above the ground state. In the intermediate state of the resonant scattering process, a Cu $1s$ electron is excited to the (for example) Cu $4p_\pi$ band, and the core hole potential reverses the balance between the $3d^9$ and $3d^{10}$ $\underline{L}$ configurations. The lowest energy state is then predominantly $\underline{1s}$ $3d^{10}$ $\underline{L}$ $4p_\pi$ and is about 7 eV lower than the anti-bonding state, $\underline{1s}$ $3d^9$ $\underline{L}$ $4p_\pi$ (Fig. 10).[48,49]

Conceptually, the process may then be thought of as follows. The incident photon excites a 1 s electron into a $4p$
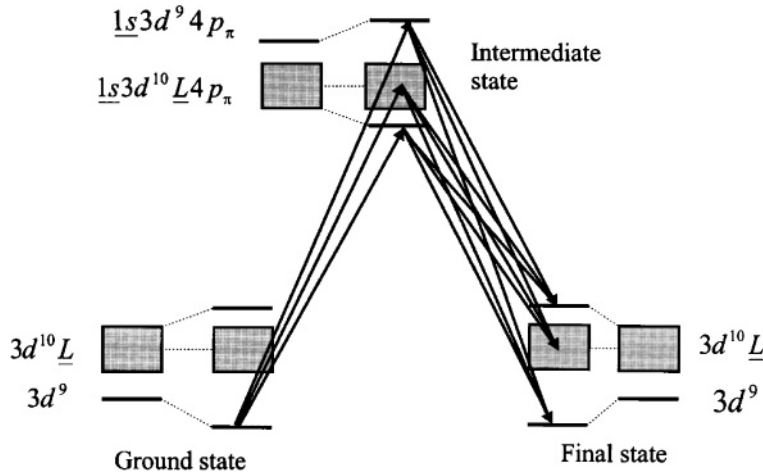
Fig. 10. Schematic energy level diagram for the resonant inelastic x-ray scattering (RIXS) process from a copper ($3d^9$) site.

band. The resulting core–hole potential shakes the system up in the intermediate state. After the core–hole decays, the system can go back down into the ground state, that is $|j\rangle = |g\rangle$, and this gives rise to elastic scattering. Importantly however, there is a finite overlap between the "shaken up" intermediate states and excited states of the system and, therefore the system can decay into one of these excited states. The outgoing photon then has an energy less than the incident photon energy by an amount equal to the energy of the excitation created in the system. It is important to note that because there is no core–hole in the final state, this excitation energy is a property of the unperturbed system and the excitation measured spectrum is therefore that of the Hamiltonian system—as is required. This process is known as resonant inelastic x-ray scattering (RIXS) and the enhancements (for certain excitations) over non-resonant inelastic scattering (in which the transition to an excited state is made directly) can be as much as two orders of magnitude.

To illustrate the power of the new technique, we present recent work on one cuprate, $CuGeO_3$.[50] $CuGeO_3$ is a charge-transfer insulator exhibiting a low-temperature spin-Peierls phase.[51] Its crystal structure consists of CuO_4 units—plaquettes—arranged in one dimensional, "edge-sharing," chains along the c-axis.[52] The crystals used in this work were grown by the floating zone technique and the data were collected at beamline 9IDB, CMC-CAT, at the Advanced Photon Source. The upstream optics consisted of a Si(111) monochromator and a flat aluminum mirror, providing an incident beam of bandwidth 1.2 eV and an incident flux of $\approx 1.3 \times 10^{11}$ ph. s^{-1}. A Si(333) channel-cut secondary monochromator (incident flux $\sim 5 \times 10^{11}$ ph. s^{-1}) was used to provide higher resolution. The scattered radiation was collected by a spherically bent, Ge(733) diced analyzer $(R = 1\,m)$, and the overall resolution of the spectrometer was 0.36 eV (FWHM).

Figure 11 shows data taken with the incident photon energy tuned to 8990 eV, the peak of the copper resonance. Three distinct excitations are observed: The charge transfer excitation at 6.4 eV (the anti-bonding state of Fig. 10), a sharp exciton-like peak at 3.8 eV (at the charge-transfer gap, Fig. 10), with a width of 0.65 eV (FWHM) and a third peak located at 1.7 eV.

We focus here on the feature at 1.7 eV. This feature exhibits no significant dispersion with momentum transfer
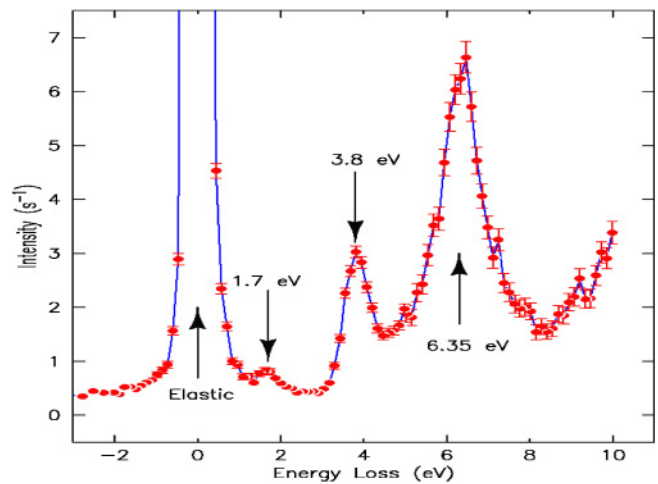

Fig. 11. (Color online) Resonant inelastic x-ray scattering data taken with the incident energy tuned to the copper K-edge of the 1D edge-sharing cuprate, CuGeO. The elastic line is resolution limited with a FWHM of 300 meV. Inelastic features are seen at 1.7, 3.8, and 6.35 eV, respectively.[50]

(not shown) and it is thus believed to result from localized d–d excitations—which are expected to have negligible dispersion [$\sim (t_{dd})^2/U \sim 1$ meV] in this system. This assignment is consistent with calculations, and with the interpretation of EELS[53,54] and optical[55–58] measurements of similar features. It is in contrast to earlier work.[59] Note that there are three non-degenerate d–d excitations possible, to (xy, yz), to xz and to y^2. These are expected to be in the range 1.41–1.76 eV, respectively.[60] With existing resolution, and absent any polarization analysis of the scattered x-ray, it is not possible to distinguish which of these excitations are contributing to the observed feature at 1.7 eV, and it is possible that it is a superposition of all three. We note that such d–d excitations have also been observed with soft x-ray RIXS experiments, where the resonance process involves excitations directly into the d-levels, greatly increasing the cross-section for such processes (see, e.g., refs. 61 and 62). A schematic illustration of one of these d–d excitations is shown in Fig. 12.

Results, such as these, reveal the power of the RIXS technique, which combines the sensitivity to electronic excitations of optical measurements with the ability to
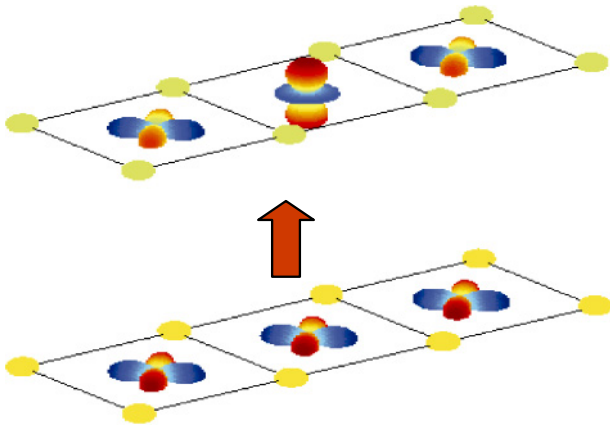
Fig. 12. (Color online) Schematic of the d–d excitation at 1.7 eV excitation in CuGeO$_3$. The $d_{x^2-y^2}$ hole on a single copper site is excited into a $d_{y^2-r^2}$ hole.[50]

transfer finite momentum and probe the dispersion of the excitations. As the resolution of such experiments continues to improve to 100 meV and below, it is clear that this technique will realize its early potential and take its place as another weapon in the arsenal of techniques employed to probe condensed matter systems. This is a prospect that Gen would have found both exciting, and we feel, irresistible.

9. Future Directions

We conclude this paper with some thoughts on future directions for magnetic x-ray scattering. The first detailed models put forward to explain the experimental observations of non-resonant[3,6,7,31] and resonant x-ray cross-sections[10] were developed more than twenty years ago. Since then, many new applications have appeared, some of which have been discussed in this paper. Nevertheless, it seems clear that some of the most exciting directions for such studies are just beginning, e.g., in resonant orbital x-ray scattering and resonant inelastic x-ray scattering, to name just two. It is a characteristic of Gen Shirane that he recognized the power of those technologies early, and with his colleagues exploited them to address a series of interesting and important questions in condensed matter physics, always driven by his desire to get to the heart of the matter.

It is a pleasure to honor Gen's memory in this small way. All of us at Brookhaven National Laboratory miss him and his remarkable enthusiasm for science.

Acknowledgement

1) R. Nathans, C. G. Shull, G. Shirane and A. Andresen: J. Phys. Chem. Solids **10** (1959) 138.
2) M. Blume: Phys. Rev. **130** (1963) 1670.
3) M. Blume and D. Gibbs: Phys. Rev. B **37** (1988) 1779.
4) J. P. Hill and D. E. McMorrow: Acta Crystallogr., Sect. A **52** (1996) 236.
5) D. Gibbs, J. P. Hill and C. Vettier: in *Third-Generation Hard X-ray Synchrotron Radiation Sources: Source Properties, Optics, and Experimental Techniques*, ed. D. M. Mills (John Wiley & Sons, Chichester, 2002). (Portions of the present text are excerpted from Chap. 8 with permission.)
6) F. de Bergevin and M. Brunel: Phys. Lett. A **39** (1972) 141.
7) M. Blume: J. Appl. Phys. **57** (1985) 3615.
8) M. Blume: in *Resonant Anomalous X-ray Scattering: Theory and Practice*, ed. G. Materlik, C. J. Sparks and K. Fischer (Elsevier Science, Amsterdam, 1994) p. 495.
9) D. Gibbs: Synchrotron Radiat. News **5** (1992) 18.
10) J. P. Hannon, G. T. Tramell, M. Blume and D. Gibbs: Phys. Rev. Lett. **61** (1988) 1245.
11) K. Namikawa, M. Ando, T. Nakajima and H. Kawata: J. Phys. Soc. Jpn. **54** (1985) 4099.
12) D. Gibbs, D. R. Harshman, E. D. Isaacs, D. B. McWhan, D. Mills and C. Vettier: Phys. Rev. Lett. **61** (1988) 1241.
13) D. B. McWhan, C. Vettier, E. D. Isaacs, G. E. Ice, D. P. Siddons, B. Hastings, C. Peters and O. Vogt: Phys. Rev. B **42** (1990) 6007.
14) J. Luo, G. T. Trammell and J. P. Hannon: Phys. Rev. Lett. **71** (1993) 287.
15) D. Gibbs, G. Grübel, D. R. Harshman, E. D. Isaacs, D. B. McWhan, D. Mills and C. Vettier: Phys. Rev. B **43** (1991) 5663.
16) J. Bohr, D. Gibbs and K. Huang: Phys. Rev. B **42** (1990) 4322.
17) P. M. Gehring, L. Rebelsky, D. Gibbs and G. Shirane: Phys. Rev. B **45** (1992) 243.
18) M. K. Sanyal, D. Gibbs, J. Bohr and M. Wolff: Phys. Rev. B **49** (1994) 1079.
19) D. B. Pengra, N. B. Thoft, M. Wulff, R. Feidenhans'l and J. Bohr: J. Phys.: Condens. Matter **6** (1994) 2409.
20) T. Thole, P. Carra, F. Sette and G. van der Laan: Phys. Rev. Lett. **68** (1992) 1943.
21) P. Carra, T. Thole, M. Altarelli and X. Wang: Phys. Rev. Lett. **70** (1993) 694.
22) P. Carra and B. T. Thole: Rev. Mod. Phys. **66** (1994) 1509.
23) J. P. Hill, C.-C. Kao and D. E. McMorrow: Phys. Rev. B **55** (1997) R8662.
24) A. Stunault, F. de Bergevin, D. Wermeille, C. Vettier, Th. Brüchel, N. Bernhoeft, G. McIntyre and J. Y. Henry: Phys. Rev. B **60** (1999) 10170.
25) W. Neubeck, C. Vettier, K. B. Lee and F. de Bergevin: Phys. Rev. B **60** (1999) R9912.
26) W. Neubeck, C. Vettier, F. de Bergevin, F. Yakhou, D. Mannix, O. Bengone, H. Alovani and A. Barbier: Phys. Rev. B **63** (2001) 134430.
27) S. Langridge, J. A. Paixao, N. Bernhoeft, C. Vettier, G. H. Lander, D. Gibbs, S. A. Sorensen, A. Stunault, D. Wermeille and E. Talik: Phys. Rev. Lett. **82** (1999) 2187.
28) D. R. Mannix, A. Stunault, N. Bemhoeft, L. Paolasini, G. H. Lander, C. Vettier, E. de Bergevin, D. Kaczorowski and A. Czopnik: Phys. Rev. Lett. **86** (2001) 4128.
29) M. van Veenendaal: Phys. Rev. B **67** (2003) 134112.
30) M. Usuda, J.-I. Igarashi and A. Kodama: Phys. Rev. B **69** (2004) 224402.
31) F. de Bergevin and M. Brunel: Acta Crystallogr., Sect. A **37** (1981) 314.
32) M. Brunel and F. de Bergevin: Acta Crystallogr., Sect. A **37** (1981) 324.
33) C. Giles, C. Malgrange, J. Goulon, F. de Bergevin, C. Vettier, A. Fontaine, E. Dartyge, S. Pizzini, F. Baudelet and A. Freund: Rev. Sci. Instrum. **66** (1995) 1549.
34) J. C. Lang and G. Srajer: Rev. Sci. Instrum. **66** (1995) 1540.
35) C. Vettier and D. B. McWhan: Physica B **159** (1989) 106.
36) V. Fernandez, C. Vettier, F. de Bergevin, C. Giles and W. Neubeck: Phys. Rev. B **57** (1998) 7870.
37) H. A. Alperin: Phys. Rev. Lett. **6** (1961) 55.
38) J. P. Hill, G. Helgesen and D. Gibbs: Phys. Rev. B **51** (1995) 10336.
39) P. G. Evans, E. D. Isaacs, G. Aeppli, Z. Cai and B. Lai: Science **295** (2002) 1042.
40) C. Detlefs, A. I. Goldman, C. Stassis, P. C. Canfield, B. K. Cho, J. P. Hill and D. Gibbs: Phys. Rev. B **53** (1996) 6355.
41) C. Detlefs, A. H. M. Z. Islam, A. I. Goldman, C. Stassis, P. C. Canfield, J. P. Hill and D. Gibbs: Phys. Rev. B **55** (1997) R680.
42) V. Scagnoli, U. Staub, A. M. Mulders, M. Janousch, G. I. Meijer, G. Hammerl, J. M. Tonnerre and N. Stojic: Phys. Rev. B **73** (2006) 100409(R).

43) J. Strempfer, Th. Brückel, U. Rutt, J. Schneider, K.-D. Liss and T. Tschentscher: Acta Crystallogr., Sect. A **52** (1996) 438.

44) A. Vigliante, M. von Zimmerman, J. R. Schneider, T. Frello, N. H. Anderson, J. Madsen and D. Buttrey: Phys. Rev. B **56** (1997) 8248.

45) M. von Zimmerman, A. Vigliante, T. Miemoller, N. Ichikawa, T. Frello, J. Madsen, P. Wochner, S. Uchida, N. H. Andersen, J. Tranquada, D. Gibbs and J. Schneider: Europhys. Lett. **41** (1998) 629.

46) J. Strempfer, Th. Brückel, D. Hupfeld, J. R. Schneider, K.-D. Liss and Th. Tschentscher: Europhys. Lett. **40** (1998) 569; J. Strempfer, Th. Briickel, D. Hupfeld, J. R. Schneider, K.-D. Liss and Th. Tschentscher: Europhys. Lett. **41** (1998) 473.

47) C.-C. Kao, C. T. Chen, E. D. Johnson, J. B. Hastings, H. I. Lin, G. H. Ho, G. Meigs, J. M. Brot, S. L. Hulbert, Y. U. Idzerda and C. Vettier: Phys. Rev. B **50** (1994) 9599.

48) J. P. Hill, A. T. Boothroyd, N. H. Andersen, E. Brecht and Th. Wolf: Phys. Rev. B **58** (1998) 11211.

49) J. P. Hill, D. E. McMorrow, A. T. Boothroyd, A. Stunault, C. Vettier, L. E. Berman, M. von Zimmermann and Th. Wolf: Phys. Rev. B **61** (2000) 1251.

50) J. P. Hill *et al.*: private conversation.

51) M. Hase, I. Terasaki and K. Uchinokura: Phys. Rev. Lett. **70** (1993) 3651.

52) H. Völlenkle, A. Wittmann and H. Nowotny: Monatsch. Chem. **98** (1957) 1352.

53) S. Atzkern, M. Knupfer, M. S. Golden, J. Fink, A. Hübsch, C. Waidacher, K. W. Becker, W. v. der Linden, M. Weiden and C. Geibel: Phys. Rev. B **64** (2001) 075112.

54) F. Parmigiani, L. Sangaletti, A. Goldoni, U. del Pennino, C. Kim, Z.-X. Shen, A. Revcolevschi and G. Dhalenne: Phys. Rev. B **55** (1997) 1459.

55) A. Damascelli, D. v. der Marel, G. Dhalenne and A. Revcolevschi: Phys. Rev. B **61** (2000) 12063.

56) S. Pagliara, F. Parmigiani, P. Galinetto, A. Revcolevschi and G. Smaoggia: Phys. Rev. B **66** (2002) 24518.

57) M. Bassi, P. Camagni, R. Rolli, G. Samoggia, F. Parmigianni, G. Dhalenne and A. Revcolevschi: Phys. Rev. B **54** (1996) R11030.

58) V. Corradini, A. Goldoni, F. Parmigiani, C. Kim, A. Revcolevschi, L. Sangaletti and U. del Pennino: Surf. Sci. **420** (1999) 142.

59) I. Terasaki, R. Itti, N. Koshizuka, M. Hase, I. Tsukada and K. Uchinokura: Phys. Rev. B **52** (1995) 295.

60) C. de Graaf and R. Broer: Phys. Rev. B **62** (2000) 702.

61) P. Kuiper, J.-H. Guo, C. Sathe, L.-C. Duda, J. Nordgren, J. J. M. Pothuizen, F. M. F. de Groot and G. A. Sawatzky: Phys. Rev. Lett. **80** (1998) 5204.

62) G. Ghiringhelli, N. B. Brookes, E. Annese, H. Berger, C. Dallera, M. Grioni, L. Perfetti, A. Tagliaferri and I. Braicovich: Phys. Rev. Lett. **92** (2004) 117406.

Martin Blume was born in New York in 1932. He obtained his A.B. degree from Princeton (1954) and his Ph. D. degree in physics from Harvard (1959) He was a Fulbright Research Fellow at the University of Tokyo (1959–1960) and a Research Associate at Harwell, UK (1960–1962). He came to Brookhaven National Laboratory in 1962 where he served in many research and administrative positions, ultimately as Deputy Director of the Laboratory. His research covered many areas in condensed matter and statistical physics, including magnetism, phase transitions, neutron and x-ray scattering, and synchrotron radiation. He was also a Professor of Physics at the State University of New York at Stony Brook (1972–1978). Since 1997 he has been Editor-in-Chief of the American Physical Society, with responsibility for all of the Physical Review journals as well as Physical Review Letters and Reviews of Modern Physics.

Doon Gibbs obtained his B.A. in physics and mathematics from the University of Utah in 1977, and his Ph. D. in physics from the University of Illinois at Urbana-Champaign in 1982. He joined Brookhaven National Laboratory in 1983 as an assistant physicist and became senior physicist in 2000. He has been the Group Leader of X-ray Scattering, (1991–2001) Associate and Deputy Chair of the Physics Department and Head of Condensed Matter (2000–2001). Gibbs is currently the Associate Laboratory Director for Basic Energy Sciences (2002–present), overseeing research in chemistry, materials science, condensed matter physics, and nanoscience at BNL. His interests include the structure and phase behavior of magnetic materials and of thin films and interfaces.

John Hill was born in Portsmouth, U.K. in 1965. He obtained his B. Sc. (1986) from Imperial College, London and his Ph. D. (1992) from M.I.T. He joined Brookhaven National Laboratory as a post-doctoral researcher in 1992, and became Group Leader of the X-ray Scattering Group in 2001. He is presently also the Experimental Facilities Division Director of the NSLS-II project and Executive Director of the Inelastic X-ray Scattering Collaborative Development Team at the Advanced Photon Source. He was awarded the Presidential Early Career Award in 1986 and is a Fellow of the American Physical Society. His research centers on understanding the ground states and excitations in strongly correlated electron systems.